International Journal of Mining and Geo-Engineering

IJMGE

IJMGE 51-1 (2017) 37–46

DOI: 10.22059/ijmge.2017.62151

Experimental and Numerical Investigation of Rock Dynamic Fracture

Aliasghar Mirmohammadlou [a*], Hossein Memarian [a], Soheil Mohammadi [b], Mohammadamin Jafari [c]

[a] *School of Mining Engineering, College of Engineering, University of Tehran, Tehran, Iran*

[b] *School of Civil Engineering, College of Engineering, University of Tehran, Tehran, Iran*

[c] *School of Civil Engineering, College of Engineering, University of Torento, Torento, Canada*

Article History:

Received 21 July 2016,

Revised 06 October 2016,

Accepted 11 November 2016.

ABSTRACT

Rapid development of engineering activities expands through a variety of rock engineering processes such as drilling, blasting, mining and mineral processing. Rock dynamic fracture mechanics methods are required to characterize the rock behavior in these activities. Dynamic fracture toughness is an important parameter for analysis of engineering structures under dynamic loading. Several experimental methods are used to determine the dynamic fracture properties of materials. Among them, the Hopkinson pressure bar and the drop weight have been frequently used to analyze the rocks properties. On the other hand, numerical simulations have been proved to be useful in dynamic fracture studies. Among various numerical techniques, the powerful extended finite element method (XFEM) enriches the finite element approximation with appropriate functions extracted from the fracture mechanics solution around a crack-tip. The main advantage of XFEM is its capability in modeling different states on a fixed mesh, which can be generated without considering the existence of discontinuities. In this paper, first, the design of a drop weight test setup was presented, and afterwards, the experimental tests on igneous (basalt) and calcareous (limestone) rocks of single-edge-cracked bend specimen were discussed. Then, each experimental test is modeled with the XFEM code. Finally, the obtained experimental and numerical results were compared. The results indicate that the experimentally predicted dynamic fracture toughness has less than 8 percent difference with the dynamic fracture toughness calculated from extended finite element method.

Keywords : *Rock fracture dynamic toughness, extended finite element method (XFEM), three point bending test, drop weight setup*

Abbreviations

K_{Id} Dynamic fracture-initiation toughness
K_{IC} Static fracture-initiation toughness
S Support span
a Crack (notch) depth
B Specimen thickness
W Specimen width
$f(a/W)$ Dimensionless stress intensity factor
N Total number of nodes
n_I Node I
N^g Set of nodes that their corresponding elements are cut by crack faces (but not crack-tip)
u_I FEM displacement vector of regular degrees of freedom
a_J Vector of additional degrees of freedom which are related to the modeling of crack faces (not crack-tips)
$b^l{}_k$ Vector of additional degrees of freedom for modeling crack-tips
ϕ_I Shape function associated with the node I
$F_l(x)$ Crack-tip enrichment functions
K Set of nodes associated with crack-tip in its influence domain
H(x) Heaviside enrichment function
Ω A body
Γ_c An initial traction-free crack
Γ_t Traction
Γ_u Displacement
Γ_c Crack boundaries
σ Stress tensor
f^b Body force
f^t External traction vectors
u^h Vector of nodal parameters (displacements u)
$\ddot{u}^h$ Vector of nodal parameters (enrichment degrees of freedom **a** and its second time derivative)
K Stiffness matrix
M Mass matrix
$B=\nabla N$ Matrix of derivatives of shape functions

1. Introduction

The knowledge of behavior of materials under dynamic fracturing at high strain rates is essential for the design components subjected to dynamic loads. This behavior is described by fracture parameters, such as the dynamic fracture-initiation toughness (K_{Id}), which represents the value of the stress intensity factor (SIF) at which a crack begins to propagate. The methodology for determination of the dynamic fracture-initiation toughness in static condition (K_{IC}) is known as the standard method for evaluating the dynamic fracture properties. However, different methods have been proposed to evaluate the dynamic fracture properties of different materials. The Hopkinson pressure bar, the Charpy impact and the drop weight test are three common techniques used for determination of dynamic fracture properties of materials. Notched three point bend specimens are used in these tests. The instrument used in the Hopkinson bar has been widely used to conduct fracture tests for measuring the dynamic fracture toughness [1, 2]. Testing of pre-cracked Charpy specimens can yield values that are

* Corresponding author. Tel.: (+98)9125987446; *E-mail address:* mirmohammadlo.aliasghar@gmail.com (A. Mirmohammadlou).

related to K_{IC} values [3]. The drop-weight machine has become a standard laboratory equipment through the ASTM standard E-208. It is possible to design many different specimen geometries to be tested in the drop-weight machine, but the most common geometries are the edge-notched specimens in a three point bend configuration [4].

Tang et al. in 1999 determined the dynamic fracture toughness of marble using cubic-shaped specimens in drop-weight test apparatus [5], while Wang et al. determined it by using holed-cracked flattened Brazilian discs and cracked straight-through fattened Brazilian discs in the Hopkinson pressure bar apparatus [6, 7]. Nikita et al. examined the static and dynamic stress intensity factors of a few different rock types [8]. Chen et al. used notched semi-circular bends and Die tested cracked chevron notched Brazilian disc and notched semi-circular bends to determine the dynamic fracture toughness of granites [9, 10, and 11]. The International Society for Rock Mechanics (ISRM) also suggested the short rod (SR) and the chevron bending (CB) tests in 1988 [12] and the cracked chevron notched Brazilian disc (CCNBD) in 1995 to determine the static toughness [13]. All the mentioned tests are core-based test to facilitate preparation of samples from natural rock mass cores. The ISRM commission on rock dynamics suggested the split Hopkinson's pressure bar (SHPB) test for measuring the dynamic fracture toughness of a rock sample using notched semi-circular bend (NSCB) specimens [14].

Modeling is essential for studying the fundamental processes occurring in rock, for assessing the anticipated and actual performance of structures built on and in rock masses, and hence for supporting rock engineering design. Also, numerical methods are used to verify laboratory results [15].The extended finite element method (XFEM) is capable of modeling strong and weak discontinuities within a standard finite element framework. In this method, analytically derived functions are added to the standard finite element approximation to reproduce the exact analytical solution. If isotropic linear elasticity is the dominant behavior, the two-dimensional asymptotic crack-tip displacement fields and a discontinuous function are usually adopted to represent a crack. This allows modeling the domain without explicitly meshing the crack surfaces, and without any re-meshing, it would facilitate crack propagation procedure on the initial mesh [16].

Dynamic fracture problems can be categorized into stationary and propagating cracks. In both cases, stress and displacement fields around the crack tip are time dependent. Chen [17] and Baker [18] studied the stress and displacement fields of dynamic stationary crack problems in isotropic materials. The stress and displacement fields of the dynamic crack propagation with high speed in isotropic materials is also studied by Freund [19], Nishioka and Atluri [20].

The dynamic crack propagation formulation and the crack tracking procedure are the main two independent parts involved a dynamic crack analysis by XFEM. The way dynamic crack propagation is formulated is related to the first part. A methodology for switching from a continuum to a discrete discontinuity was developed by Belytschko et al. [21], based on the loss of hyperbolicity for rate independent materials. The loss of hyperbolicity was further studied by Gao and Klein [22], Peerlings et al. [23] and Oliver et al. [24]. The second part is a crack tracking procedure to represent an existing crack and its evolution by time. The level set and fast marching methods are available. They have been successfully implemented in the XFEM codes and can be used for efficient quasi-static or dynamic crack evolution problems (2003).

In this paper, rock dynamic fracture is studied experimentally and numerically. First of all, we describe the apparatus (developed at University of Tehran) that determines the dynamic fracture properties of materials and the procedure of determining the dynamic fracture toughness. Then, the test results of three point specimens for igneous (basalt) and calcareous (limestone) rocks are discussed. Finally, by performing the extended finite element modeling, the results of experimental and numerical dynamic fracture toughnesses are compared.

2. Experimental processes

2.1. Experimental setup for determination of dynamic fracture

Although most researchers use Hopkinson's machine for dynamic tests, the drop weight test machine has been utilized here for two main reasons:

1) The specimens of Hopkinson's machine are smaller. This difference in dimensions significantly affects the test results due to the increased effect of inhomogeneity in larger specimens. Discontinuities and micro-cracks naturally occurring in rocks are more likely to be incorporated in larger specimens (40 cm) than smaller ones (2-3 cm), and therefore, constitute a significant change in dynamic behavior. Consequently, larger dimensions represent a better and more realistic description.
2) Whereas Hopkinson's component for impact application is already in contact with the specimen even before exertion of the load, the drop system applies the load to the specimen in a natural manner so that the impact has an initial velocity and a real dynamic loading is in effect.

This paper describes an experimental technique for studying the dynamic fracture toughness of rocks. Based on the impact testing machine constructed at University of Tehran, a three point bending specimen is fractured under impact loading (Figure 1).

In this machine, the load P can be measured during the impact. The main components of the machine include: elastic steel bar with 1500 mm in length and 30 mm in diameter, supports, drop system, base and the data acquisition system. Since the load acting on the specimen measures the dynamic fracture toughness, it is determined by the output of the strain gauges mounted on the bar (Figure 2a). Effects of the tub shape on rock fracture parameters have not been studied, yet. Therefore, the ASTM Standard E-23 was adopted for designing the tub. The data acquisition system consists of a digital oscilloscope DS 1064 B that has four channels with 2Gsa/s sampling precision and an electrical circuit comprising an amplifier and a wheatstone bridge (Figure 2b). Considering that the output of the oscilloscope is reported in voltage, calibration is required to determine an appropriate relationship between the impact force and the reported voltage. It should be noted that the steel bar was tensioned, and then in different loads, the corresponding strains and voltages were recorded to obtain the relationship between the force and voltage.

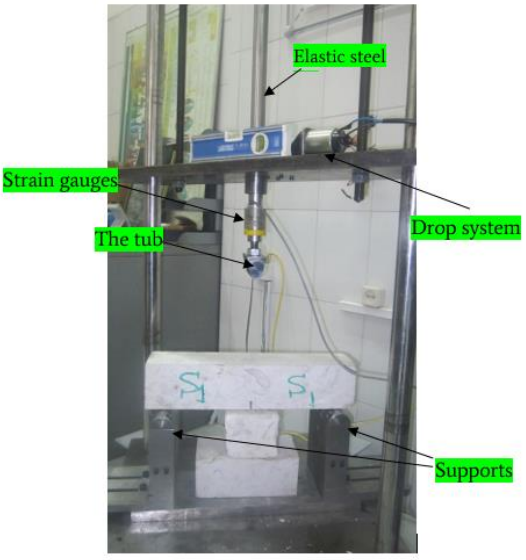

Fig. 1. Impact testing machine.

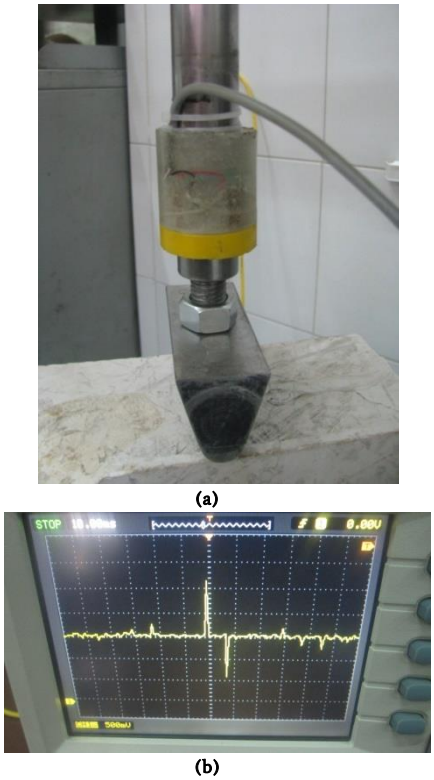

Fig.2 (a) Tub and strain gauges mounted on the bar, (b) oscilloscope for recording the load data.

This Machine has the same advantage as Hopkinson's which offers the possibility of mounting a strain gauge on the drop system. Furthermore, it has the advantageous capability of realistic impact modeling of larger specimens; but compared with Hopkinson's, it has limitations in making accurate adjustments to the quantity of applied forces. The design process for an accurate load adjustment apparatus is in progress. After production, this device will be incorporated in future designs. Another advantageous factor to this machine is its capability of performing tests on specimens in a variety of forms, including cubic, cylindrical, disc-shaped, shotcrete or concrete panels. It is acknowledged that the main issue with the drop weight test is its inertial force of impact. Examinations revealed that is case the specimen is lightweight, it will rebound off the support frame (modeled with Abaqus™ software). However, the dimensions and weight of the specimens in this machine are great enough to prevent such rebounds during the test.

2.2. Lithological details in thin sections of studied rocks

The two rock types used in this study were calcareous and igneous rocks. In specimen selection, the principal importance was given to homogeneity; hence, basalt and limestone respectively represent igneous and sedimentary rocks in this study. Furthermore, in order to acquire accurate data, two thin sections were prepared and examined under microscope. The result of these studies indicate that the calcareous rock is a bioclastic wackestone with a microcrystalline groundmass containing bioclasts such as, skeletal grans and fossil relicts (undifferentiated), mostly changed into calcite cement casts. Also, the fractures of 0.5 - 2.0 mm thick were completely filled by sparry calcite cement (Fig.3a). The igneous rock, on the other hand, is an unaltered basalt with a vitreous groundmass and plagioclase phenocrysts (Fig.3b).

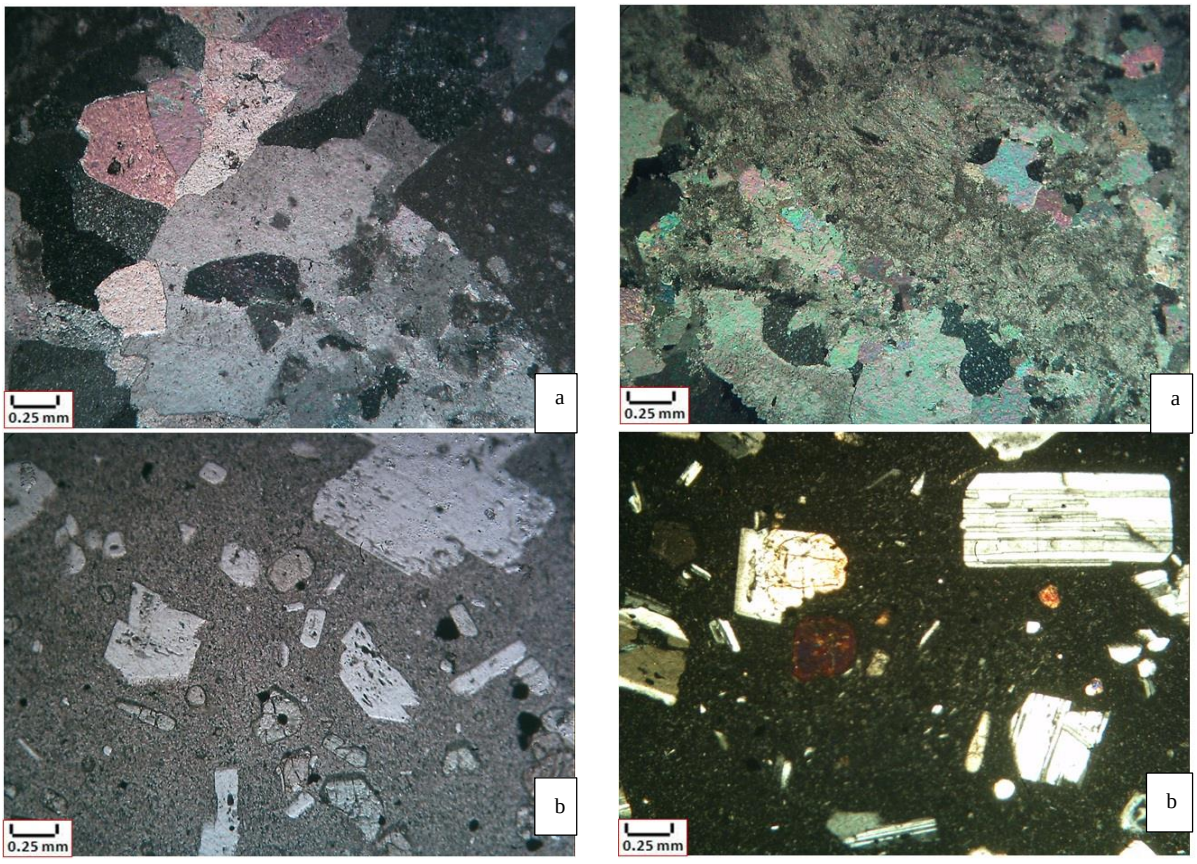

Fig. 3. The photomicrographs of studied this sections of selected rocks. (a) calcareous (bioclastic wackestone), (b) igneous (basalt).

Despite its compatibility with various shapes and dimensions of specimens, larger specimens were tested in this study as much as possible. The most common form in such machines is the notched cubic specimens. In order to determine the elastic modulus and the Poison ratio of basalt, uniaxial tests were carried out. Furthermore, in order to carry out mode I tests, five notched cubic specimens were prepared with notches in the middle. The notches were 2mm wide with different depths and the same span lengths. Dimensions of specimens and spans are given in Table 1. Where, S is the support span; a is the crack (notch) depth; B is the specimen thickness; W is the specimen width.

Comparing the failure surfaces of fractured specimens, it is apparent that failure surfaces of calcareous (limestone) specimens are rougher than igneous (basalt) rocks. Therefore, compared to limestone, basalt is a homogenous rock (Fig.5). These details was not included in the numerical modeling due to greater emphasis on the more general properties of the rock specimens.

Table 1. Dimensions of specimens.

Sample No	Rock Type	B(mm)	W(mm)	a	S(mm)
S_1	Limestone	105	100	20	380
S_2		105	100	18	380
S_3		105	100	20	380
S_4	Basalt	105	100	15	380
S_5		105	100	30	380

2.3. Test Results

Fig.4 shows the specimens before and after the tests. Obviously, all specimens were fractured under the pure state of mode I and the cracks propagated vertically. The graph for the applied force to each specimen was recorded by an oscilloscope for each test. After each test, the fracture surface was thoroughly examined.

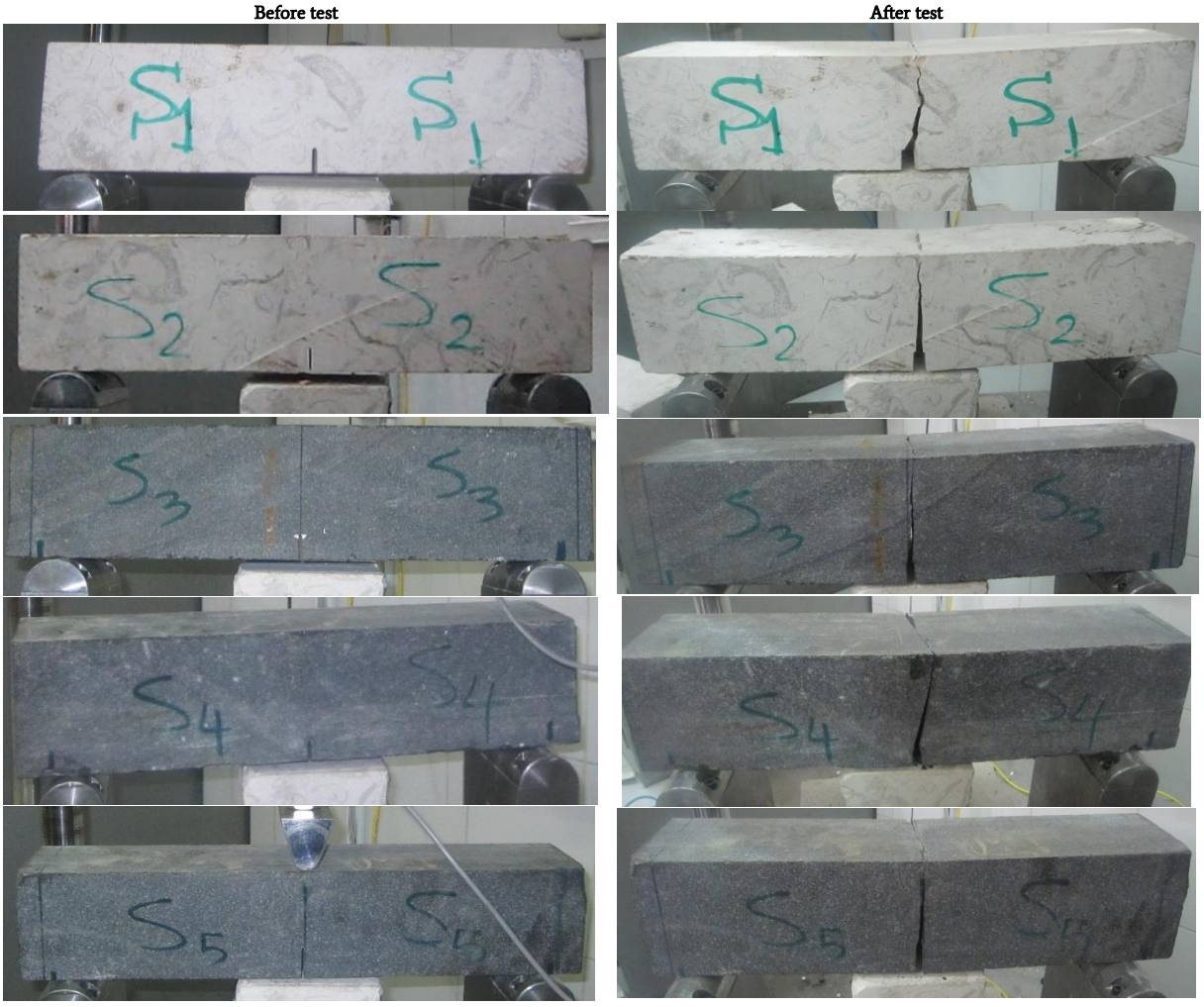

Fig.4: Specimens before and after tests

2.4. Determination of dynamic fracture toughness from experimental

Dynamic fracture toughness can be calculated by applying the following equation (Tang et al) [5]:

$$K_{Id} = \frac{P_Q . S}{B . W^{3/2}} * f(a/w) \quad (1)$$

Where P_Q is force value; S is the support span; a is the crack (notch) depth; B is the specimen thickness; W is the specimen width; and $f(a/w)$ is the dimensionless stress intensity factor, defined by Eq. (2). Results for each specimen are presented in Table 2.

$$f(a/w) = (\frac{a}{w})^{1/2} \times \left[2.9 - 4.6\left(\frac{a}{w}\right) + 21.8\left(\frac{a}{w}\right)^2 - 37.6\left(\frac{a}{w}\right)^3 + 38.7(\frac{a}{w})^4\right] \quad (2)$$

As described in section 2.1, the most important experimental data is impact load. Impact load is calculated by strain gauge that was installed on the bar. Dynamic force is applied to the samples and the length of bar changes under the implied force.This length shortening leads to voltage variation on the oscilloscope. By using the calibration equation,

the force is obtained.

Table 2 $f(a/w)$ for specimens

Sample No	$f(a/w)$
S_1	1.168
S_2	1.103
S_3	1.168
S_4	1.004
S_5	1.523

P_Q was determined based on data collected by the oscilloscope (Table 3). As the results show, maximum and minimum impact force is respectively for igneous and calcareous rock.

Table 3 Impact forces for specimens

Sample No	P_Q(N)
S_1	64239.7
S_2	27325.7
S_3	101153.7
S_4	55011
S_5	78082

The dynamic fracture toughness calculated from Eq. (1), are given in Table 4.

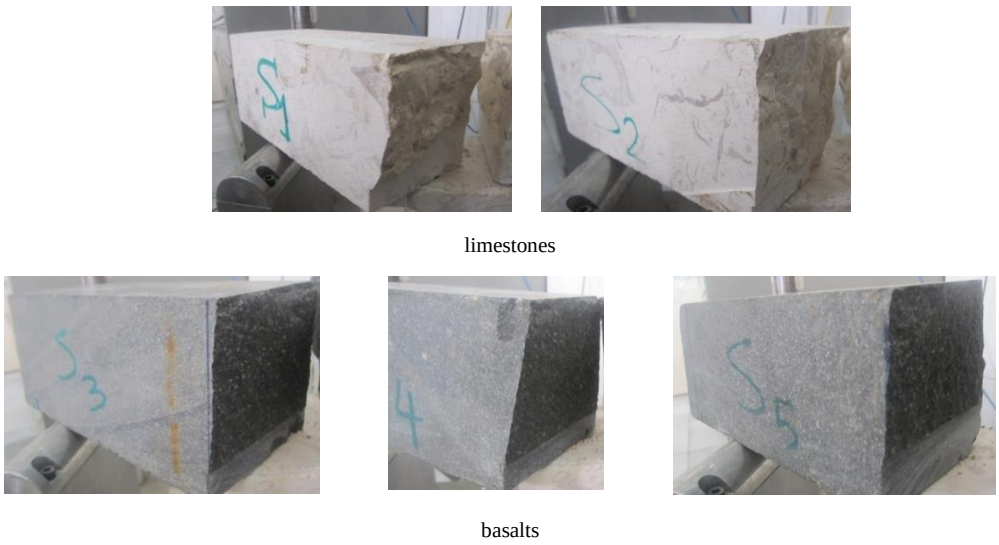

Fig.5: Fractured surfaces of limestones and basalts specimens under dynamic loading

Table 4 Experimental dynamic fracture toughness

Sample No	K_I_Exp(MPa.m$^{1/2}$)
S_1	8.59
S_2	3.45
S_3	13.53
S_4	5.74
S_5	12.2

The dynamic fracture toughness depends on loading, and therefore, different results (dynamic fracture toughness) were obtained for each rock.

Generally, the toughness of basalt is greater than that of limestone and this is due to denser distribution of planes of weakness in limestone. Based on the results of these experiments, it is concluded that increased inhomogeneity in rocks produces greater irregularity and roughness in fracture surfaces. In a parallel manner, homogeneous rocks are expected to produce regular and uniform fracture surfaces. Thorough investigation of this issue can provide the possibility of inducing predetermined and desired fracture surfaces in rock structures.

3. Numerical evaluation for dynamic fracture

3.1. Basics of XFEM

In XFEM, the finite element mesh is generated regardless of the existence and location of any cracks. Then, through the use of level set or other search algorithms, the exact location of any discontinuity is determined with respect to the existing mesh. Afterwards, a few degrees of freedom are added to the classical finite element model in selected nodes around the discontinuity. These additional degrees of freedom contribute to the approximation through the use of the generalized Heaviside and crack-tip (near-tip) functions. Assume a discontinuity (a crack) within an independent finite element mesh, as depicted in Fig. 6. The displacement field for any typical point x inside the domain can be written in terms of the classical finite element approximation and the XFEM enriched fields (Eq. (3)) [25, 26]:

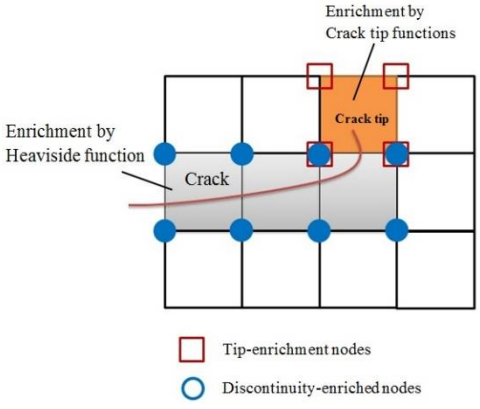

Fig.6 Determining the elements and nodes for discontinuity and crack tip enrichments [25].

$$\boldsymbol{u}^h(x) = \sum_{n_I \in N} \phi_I(x)\boldsymbol{u}_I + \sum_{n_J \in N^g} \phi_J(x)H(x)\boldsymbol{a}_J + \sum_{k \in K} \phi_k(x)\left(\sum_l F_l(x)\boldsymbol{b}_k^l\right) \quad (3)$$

where N is the total number of nodes, n_I represents the node I, N^g is the set of nodes that their corresponding elements are cut by crack faces (but not crack-tip), u_I is the FEM vector of regular degrees of freedom, a_J is the vector of additional degrees of freedom which are related to the

modeling of crack faces (not crack-tips), b^l_k is the vector of additional degrees of freedom for modeling crack-tips, ϕ_I is the shape function associated with the node I, $F_l(x)$ are the crack-tip enrichment functions and K are the set of nodes associated with crack-tip in its influence domain. H(x) is the Heaviside enrichment function:

$$H(x) = \begin{cases} +1 & if\ (x - x^*).e_n > 0 \\ -1 & otherwise \end{cases} \quad (4)$$

The crack-tip enrichment functions are obtained from the analytical solution for displacement in the vicinity of a crack-tip.

$$\{F_l(r.\theta)\}_{l=1}^4 = \left\{\sqrt{r}cos\frac{\theta}{2}.\sqrt{r}cos\frac{\theta}{2}.\sqrt{r}sin\frac{\theta}{2},\sqrt{r}sin\frac{\theta}{2}\right\} \quad (5)$$

3.2. Dynamic XFEM

Consider a body Ω with an initial traction-free crack Γ_c in the state of dynamic equilibrium. The fundamental elastodynamic equation can be expressed as [27]:

$$\nabla.\sigma + f^b = \rho\ddot{u} \quad (6)$$

with the following boundary conditions:

$$u(x.t) = \bar{u}(x.t)\ \ on\ \Gamma_u \quad (7)$$

$$\sigma.n = f^t \quad on\ \Gamma_t \quad (8)$$

$$\sigma.n = 0 \quad on\ \Gamma_c \quad (9)$$

and initial conditions:

$$u(x.t=0) = \bar{u}(0) \quad (10)$$

$$\dot{u}(x.t=0) = \bar{\dot{u}}(0) \quad (11)$$

where Γ_t, Γ_u and Γ_c are traction, displacement and crack boundaries, respectively; σ is the stress tensor and f^b and f^t are the body force and external traction vectors, respectively. The variational formulation of the initial/boundary value problem of Eq. (6) can be written as:

$$\int_\Omega \rho\ddot{u}.\delta u\, d\Omega + \int_\Omega \sigma.\delta\varepsilon\, d\Omega = \int_\Omega f^b.\delta u\, d\Omega + \int_\Omega f^t.\delta u\, d\Gamma \quad (12)$$

In the extended finite element method, approximation is utilized to calculate the displacement $u^h(x)$ for a typical point x (Eq. (3)). The discretized form of Eq. (12) and using the XFEM procedure Eq. (6) can be written as:

$$M\ddot{u}^h + Ku^h = f \quad (13)$$

where u^h and $\ddot{u}^h$ denote the vector of nodal parameters (displacements u and enrichment degrees of freedom **a** and its second time derivative, respectively:

$$u^h = \{u.a.b\}^T \quad (14)$$

The stiffness matrix K, mass matrix M and the external load vector f are defined as:

$$K_{ij} = \begin{bmatrix} K_{ij}^{uu} & K_{ij}^{ua} \\ K_{ij}^{au} & K_{ij}^{aa} \end{bmatrix} \quad (15)$$

$$M_{ij} = \begin{bmatrix} M_{ij}^{uu} & M_{ij}^{ua} \\ M_{ij}^{au} & M_{ij}^{aa} \end{bmatrix} \quad (16)$$

$$f_i = \{f_i^u.f_i^a\}^T \quad (17)$$

where the stiffness components K_{ij}^{uu}, K_{ij}^{ua} and K_{ij}^{aa} associated with the classical FEM, coupled and enrichment parts of XFEM approximation, respectively, can be defined:

$$K_{ij}^{uu} = \int_\Omega (B_i^u)^T D B_j^u d\Omega \quad (18)$$

$$K_{ij}^{ua} = \int_\Omega (B_i^u)^T D B_j^a d\Omega \quad (19)$$

$$K_{ij}^{aa} = \int_\Omega (B_i^a)^T D B_j^a d\Omega \quad (20)$$

where B=∇N is the matrix of derivatives of shape functions. Classical and enrichment components of the consistent mass matrix can be expressed as:

$$M_{ij}^{uu} = \int_\Omega \rho N_i N_j d\Omega \quad (21)$$

$$M_{ij}^{ua} = M_{ij}^{au} = \int_\Omega \rho N_i(N_j\psi_j) d\Omega \quad (22)$$

$$M_{ij}^{aa} = \int_\Omega \rho N_i\psi_i(N_j\psi_j) d\Omega \quad (23)$$

Finally the force vectors associated with the classical and enrichment degrees of freedom are defined as:

$$f_i^u = \int_{\Gamma_t} N_i f^t d\Gamma + \int_{\Omega^e} N_i f^b d\Omega \quad (24)$$

$$f_i^a = \int_{\Gamma_t} N_i\psi f^t d\Gamma + \int_{\Omega^e} N_i\psi f^b d\Omega \quad (25)$$

The well-known newmark time integration scheme was adopted in this study.

3.3. Verification of numerical simulation

In order to verify the proposed numerical simulation, a set of tests by Rubio and et al [28] were examined. They presented a procedure to evaluate dynamic fracture-initiation toughness based on dynamic fracture tests performed on Three Point Bending specimens, in conjunction with a high-speed photography technique for direct measurement of crack mouth opening displacement (CMOD). They calculated the dynamic SIF by three different experimental methods, 1) input load 2) displacement of load point and 3) CMOD, and concluded the best way to estimate the dynamic fracture-initiation toughness is from the CMOD method. Dimensions and mechanical properties of the Rubio's specimen are summarized in Tables 5 and 6. Crack is located vertically in the center of the model.

Table 5 Dimensions for the aluminum alloy specimen [27]

Material	Width (mm)	Thickness(m m)	Length (mm)	Crack length (mm)
Aluminum alloy	20	10	90	10.8

Table 6 Mechanical properties for the aluminum alloy specimen [27]

Material	Young's Modulus(GPa)	Poisson's Ratio	Density (kg/m^3)
Aluminum alloy	72	0.3	2800

Results of the XFEM analyses were compared with the reference. Experimental tests in Fig.7 show a good conformity with the SIFs predicted by the CMOD test results.

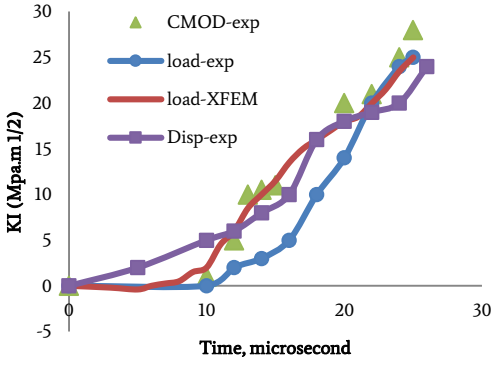

Fig.7 Comparison of experimental and numerical SIFs for the aluminum alloy specimen

3.4. Numerical modeling of the rock tests

Numerical modeling of the performed experimental tests are discussed in this section. Dynamic analyses of stationary and dynamic crack (whether the crack has propagation or not) were performed to determine the dynamic toughness. Fig.8 shows the schematic definition

of the model.

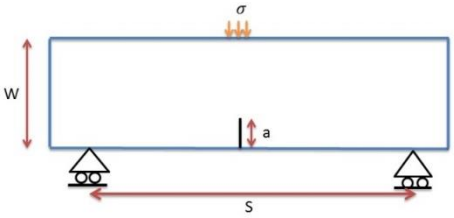

Fig.8 Schematic figure of model.

In order to verify the results of the tests, all tests on basalt rock S_3, S_4 and S_5 were modeled with numerical code. In the numerical model, a uniform mesh comprising 300×81 elements respectively in x direction and y direction was used (Fig. 9). According to the measurements of impact forces in experimental tests, the time dependent forces of Fig. 10 were applied on the model of S_3, S_4 and S_5 specimens, respectively.

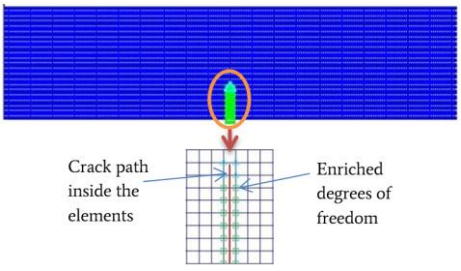

Fig.9 Finite element mesh of the model

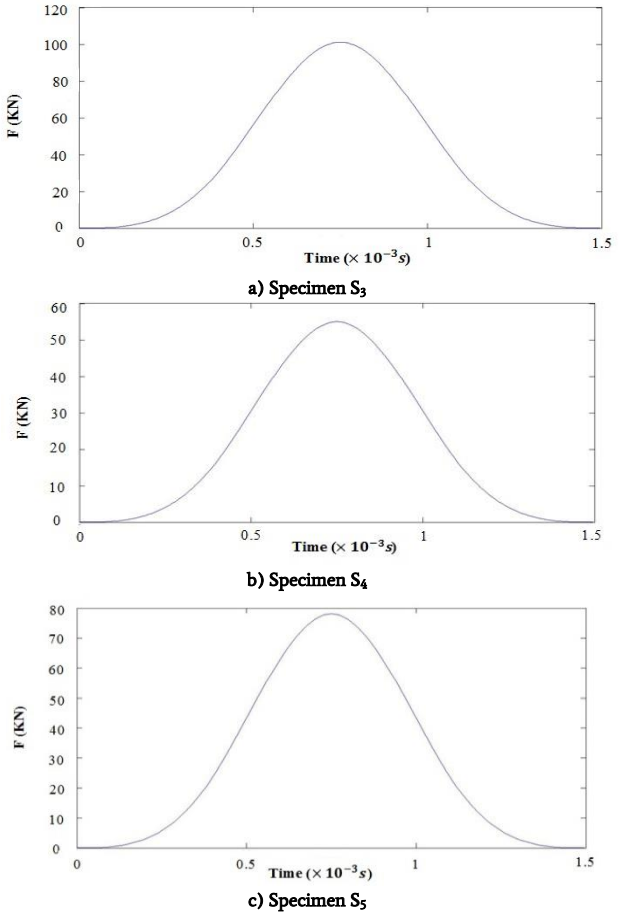

Fig.10 Time dependent impact force for the specimens, a) Specimen S3 , b) Specimen S4 , c) Specimen S5.

Mechanical characteristics of the basalt specimens are summarized in Table 7. The numerically predicted dynamic fracture toughnesses for samples of S_3, S_4 and S_5 were compared with the test results which are given in Table 8. The maximum difference was limited to less than 8 percent. In addition, $\boldsymbol{\sigma_{yy}}$, $\boldsymbol{\sigma_{xx}}$ and $\boldsymbol{\sigma_{xy}}$ stress contours for the S_3 specimen in several times of modeling are illustrated in Figs. 11-13.

Table 7: Mechanical characteristics of basalts

E (GPa)	ϑ	$\rho(\frac{kg}{m^3})$
74.8	0.17	2700

Table 8: Dynamic fracture toughness for samples S3, S4 and S5

Sample No	P_Q(N)	K_I_Num (MPa.m$^{1/2}$)	K_I_Exp (MPa.m$^{1/2}$)	Difference (%)
S_3	101153.7	13.56	13.53	1
S_4	55011	6.2	5.74	7
S_5	78082	13.3	12.2	8

Fig.14 shows vertical propagation of crack for each specimen. It can be seen that dynamic crack propagation modeling is consistent with experimental results (Fig.14).

4. Comparison of experimental and numerical results

To ensure the validity of experimental results, the values of dynamic fracture toughness in Table 4 were compared with that of numerical simulations. Furthermore, the XFEM codes utilized in these analyses were verified by exact solutions of fracture mechanics and proved to be reliable for comparison of results. Despite its inertial impact deficiencies, if the experimental results do not deviate from numerical calculations, it can be concluded that this machine is capable of yielding correct results. Experimental and numerical results and their differences are summarized in Table 9 and there is less than 8% difference between results.

Table 9 Compare experimental and numerical dynamic fracture toughness

Sample No	K_I_Exp (MPa.m$^{1/2}$)	K_I_Num (MPa.m$^{1/2}$)	Differents (%)
S_3	13.53	13.56	1
S_4	5.74	6.2	7
S_5	12.2	13.3	8

The difference between the experimental and numerical results is approximately 8 percent, which was already anticipated due to the restrictions applied to fracture growth in numerical models. This constrain was applied to prevent the excessive fluctuations of stress intensity factor during the fracture growth which renders an impossible measurement of toughness.

5. Conclusion

This research used a drop-weight testing technique on single-notched three point bend specimens to measure the mode I of dynamic fracture toughness of rock. It is believed that Hopkinson's machine is not suited for dynamic fracture tests on specimens with larger dimensions and therefore leading researchers toward drop-weight testing systems. Greater weight of such specimens eliminates the possibility of using the Hopkinson's machine. Moreover, Hopkinson's machine occupies more space whereas the drop-weight system fits in smaller spaces. It is emphasized that the advantageous points of Hopkinson's machine can be adopted by other dynamic fracture testing machines.

The experimental tests were performed on the igneous (basalt) and calcareous (limestone) rocks and the dynamic fracture toughness was calculated for each specimen. The igneous (basalt) rocks have higher value of the dynamic fracture toughness than the calcareous (limestone) rocks.

In order to ensure the validity of experimental results, the XFEM numerical code, mostly suited to fracture mechanics was utilized. The accuracy of XFEM codes was verified by the results of analytical solutions. The dynamic XFEM numerical method was adopted to simulate the test procedure and to numerically determine the dynamic fracture toughness. Finally, experimental and numerical results were compared, reporting a maximum difference of less than 8%, which is quite acceptable for such a complicated engineering problem.

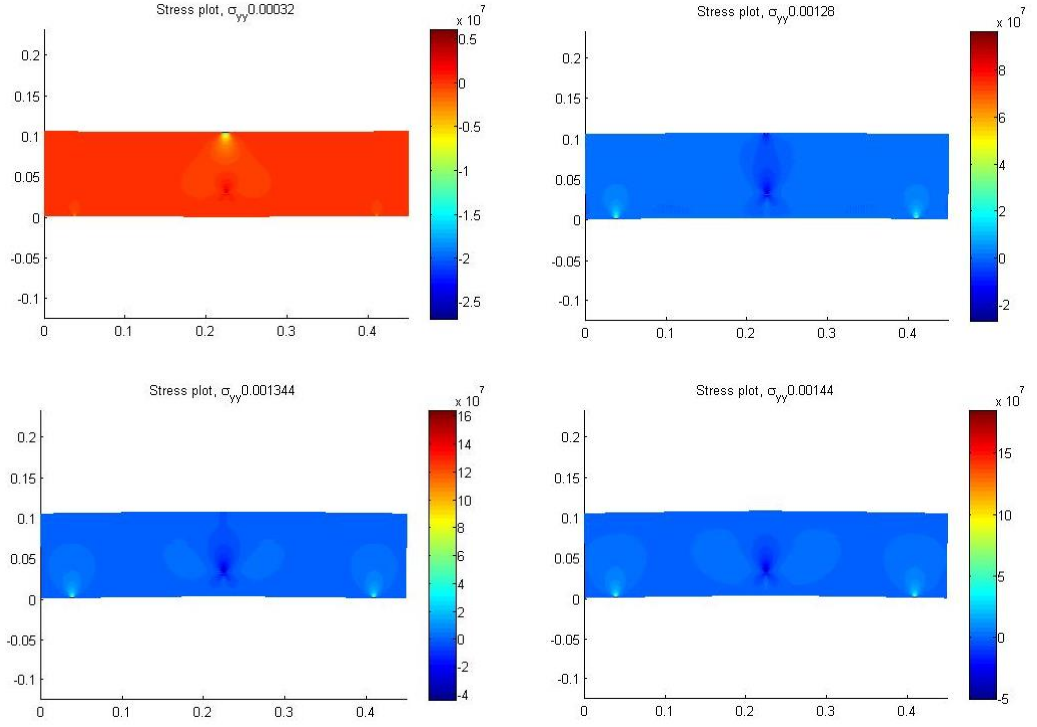

Fig.11 Contours of the σ_{yy} stress at different time steps.

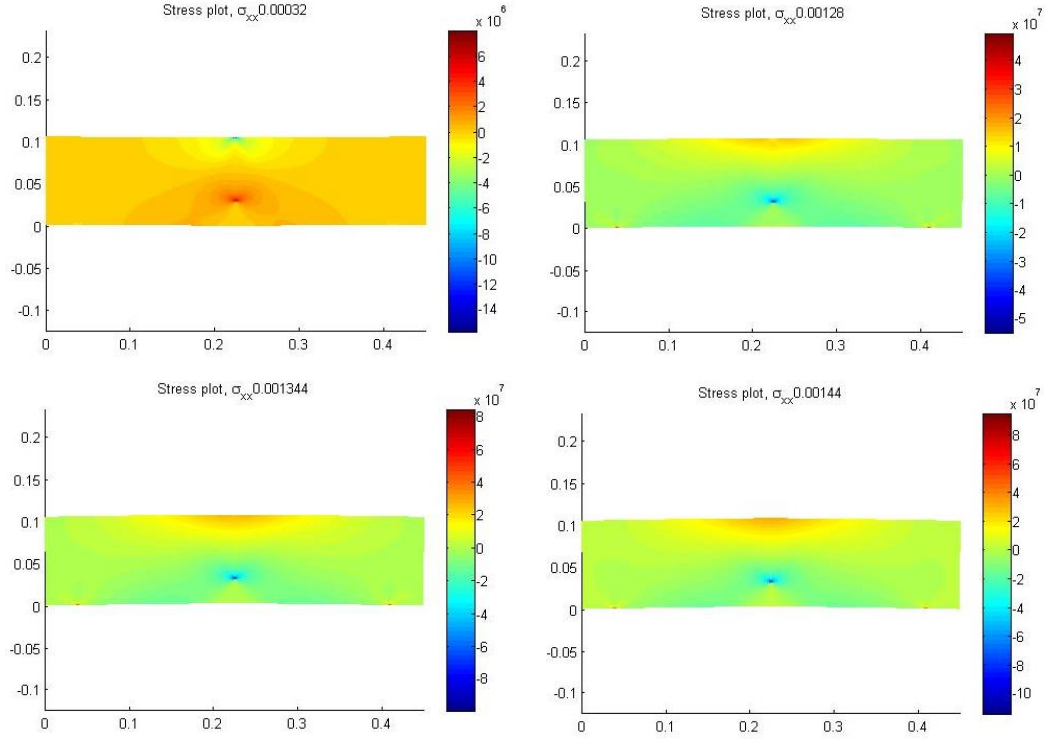

Fig.12 Contours of the σ_{xx} stress at different time steps.

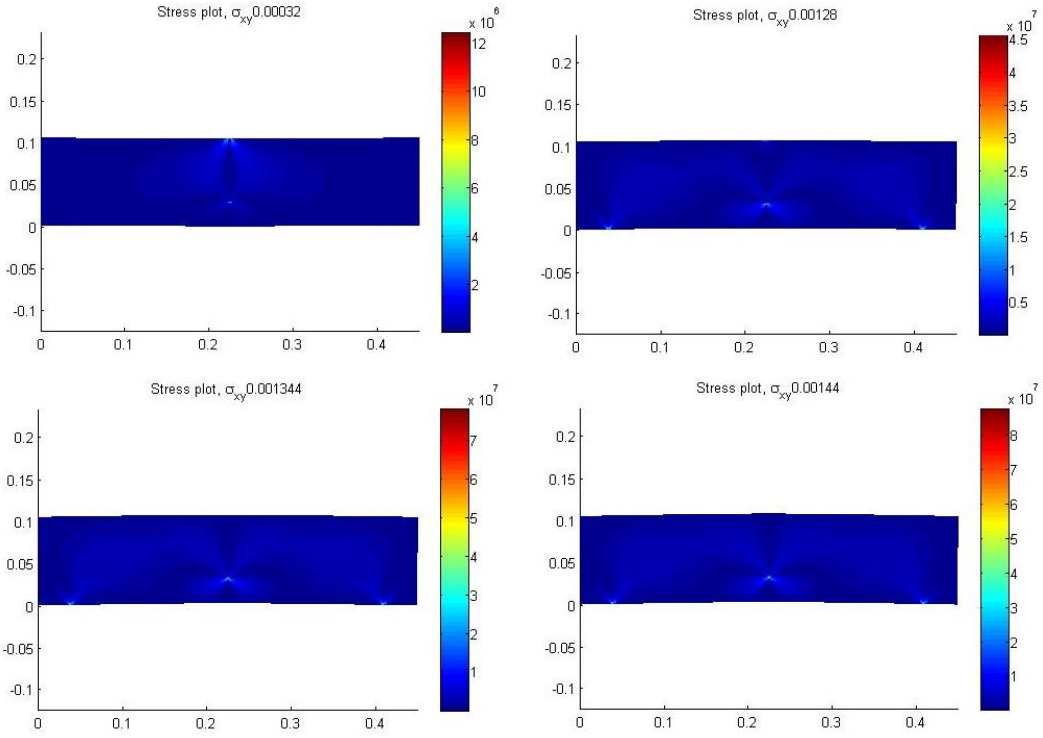

Fig.13 Contours of the σ_{xy} stress at different time steps.

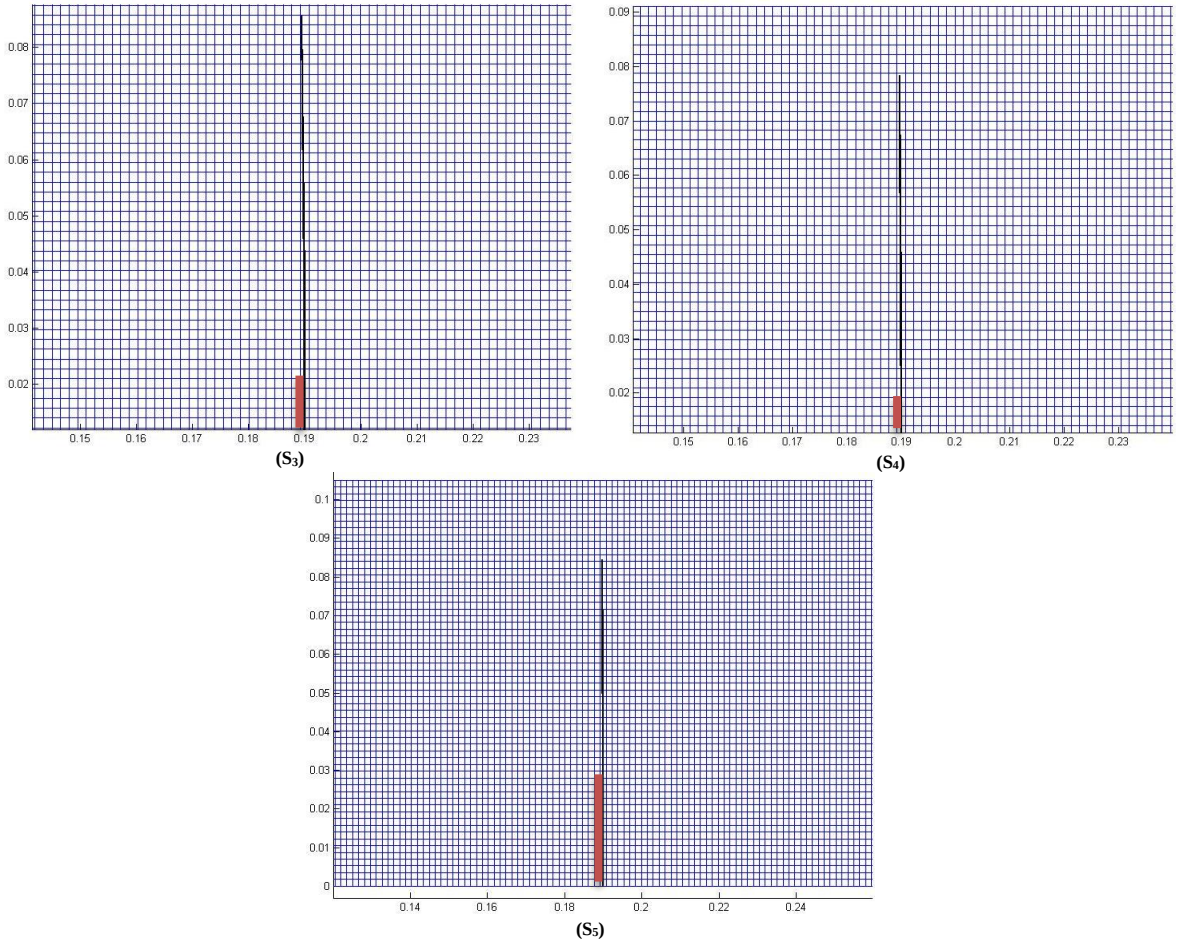

Fig.14 Crack propagation path for basalt specimens.

Acknowledgment

The authors acknowledge the geological engineering Lab, school of Mining Engineering, University of Tehran for financial support of constructing the impact testing machine and performing the tests. The numerical support of the High Performance Computing Lab, school of Civil Engineering, University of Tehran is appreciated, as well.

REFRENCES

[1] Field, J.E., Walley, S.M., Proud, W.G., Goldrein, H.T, Siviour, C.R., (2004) Review of experimental techniques for high rate deformation and shock studies, International Journal of Impact Engineering, 30, 725–775.

[2] Chunhuan, Guo., Fengchun, Jiang., Ruitang, Liu., Yang, Yang., (2011) Size effect on the contact state between fracture specimen and supports in Hopkinson bar loaded fracture test, International Journal Fracture, 169, 77–84.

[3] Sheikh, A. K., Arif, A.F.M., Qamar, S.Z., (2002) Determination of fracture toughness of tool steels, The 6th Saudi Engineering Conference, KFUPM, Dhahran, December; Vol 5, 169.

[4] Ravi-Chandar, K., (2004) Dynamic Fracture, Elsevier press.

[5] Tang, Chunan., and Xu, Xiaohe., (1999) A new method for measuring dynamic fracture toughness of rock, Engineering fracture mechanics, 35, 783-791.

[6] Wang, Q.Z., Zhang, S., Xie, H.P.,(2008) Rock Dynamic Fracture Toughness Tested with Holed-cracked Flattened Brazilian Discs, Proceedings of the XIth International Congress and Exposition, Orlando, Florida USA,50, 877-885.

[7] Wang, Q.Z., Feng, F., Ni, M., Gou, X.P., (2011) Measurement of mode I and mode II rock dynamic fracture toughness with cracked straight through flattened Brazilian disc impacted by split Hopkinson pressure bar, Engineering Fracture Mechanics,78, 2455–2469.

[8] Nikita, F. Morozov., Yuri, V. Petrov., Vladimir, I. Smirnov., (2009) Dynamic Fracture of Rocks, 7th EUROMECH Solid Mechanics Conference, Lisbon, Portugal.

[9] Chen, R., Xia, K., Dai, F., Lu, F., Luo, S.N., (2009) Determination of dynamic fracture parameters using a semi-circular bend technique in split Hopkinson pressure bar testing, Engineering Fracture Mechanics, 76, 1268–1276.

[10] Dai, F., Chen, R., Iqbal, M.J., Xia, K.,(2010) Dynamic cracked chevron notched Brazilian disc method for measuring rock fracture parameters, International Journal of Rock Mechanics & Mining Sciences, 47, 606–613.

[11] Dai, F., Xia, K., Zheng, H., Wang, Y.X., (2011) Determination of dynamic rock Mode-I fracture parameters using cracked chevron notched semi-circular bend specimen, Engineering Fracture Mechanics, 78, 2633–2644.

[12] Ouchterlony, F., (1988) Suggested methods for determining the fracture toughness of rock, International Journal Rock Mech Min Sci Goemech Abstr, 25, 71–96.

[13] Fowell, R.J., Hudson, J.A., Xu, C., Chen, J.F., (1995) Suggested method for determining mode-I fracture toughness using cracked chevron-notched Brazilian disc (CCNBD) specimens. International Journal Rock Mechanic Min Sci Goemech Abstr, 32(1), 57–64.

[14] Zhou, Y.X., Xia, K., Li, X.B., Li, H.B., Ma, G.W., Zhao, J., Zhou, Z.L., Dai, F., (2012). Suggested methods for determining the dynamic strength parameters and mode-I fracture toughness of rock materials, International Journal of Rock Mechanics & Mining Sciences, 49, 105–112.

[15] Jing, L., Hudson, J.A., (2002) Numerical methods in rock mechanics, International Journal of Rock Mechanics & Mining Sciences, 39, 409–427

[16] Sukumar, N., Prévost, J.H., (2003) Modeling quasi-static crack growth with the extended finite element method Part I: Computer implementation, International Journal of Solids and Structures, 40, 7513-7537.

[17] Chen, EP., (1978) Sudden appearance of a crack in a stretched finite strip. Journal Appl Mech, 45, 270–80.

[18] Baker, B.R. (1962) Dynamic stresses created by a moving crack. Journal Appl Mech, 29, 449–545.

[19] Freund, L.B., (1976) Dynamic crack propagation. In: Erdogan, F, editor, Mechanics of fracture. ASME, 105–34.

[20] Nishioka, T., Atluri, S.N., (1983) Path-independent integrals, energy release rates and general solutions of near tip fields in mixed-mode dynamic fracture mechanics. Eng Fract Mech, 18, 1–22.

[21] Ventura, G., Budyn, E., Belytschko, T., (2003) Vector level sets for description of propagating cracks in finite elements. International Journal Numerical Methods Eng, 58, 1571–92.

[22] Gao, H., Klein, P., (1998) Numerical simulation of crack growth in an isotropic solid with randomized internal cohesive bonds. Journal Mech Phys Solids,42(6), 187–218.

[23] Peerlings, R.H.J., de Borst, R., Brekelmans, W.A.M., Geers, M.G.D., (2002) Localisation issues in local and nonlocal continuum approaches to fracture. Eur Journal Mech A, Solids, 21, 175–89.

[24] Oliver, J., Huespe, A.E., Pulido, M.D.G., Samaniego, E., (2003) On the strong discontinuity approach in finite deformation settings. International Journal Numerical Methods Eng, 56, 1051–82.

[25] Belytschko, T., Black, T., (1999) Elastic crack growth in finite elements with minimal remeshing. International Journal Numerical Methods Eng, 45, 601–20.

[26] Mos, N., Dolbow, J., Belytschko, T., (1999) A finite element method for crack growth without remeshing. International Journal Numerical Methods Eng, 46, 131–50.

[27] Mohammadi, Soheil., (2008) Extended Finite Element Method for Fracture Analysis of Structures. Blackwell Publishing Ltd. ISBN: 978-1-4051-7060-4.

[28] Rubio, L., Fernandez-Saez, J., Navarro, C., (2006) Determination of Dynamic Fracture initiation Toughness using Three-point Bending Tests in a Modified Hopkinson Pressure Bar, Experimental Mechanics.